ACS APPLIED MATERIALS & INTERFACES

Research Article

www.acsami.org

Processing–Structure–Property Correlations of Polyethersulfone/Perfluorosulfonic Acid Nanofibers Fabricated via Electrospinning from Polymer–Nanoparticle Suspensions

Pei-Pei Lu,[†,‡] Zhen-Liang Xu,*[,†,‡] Hu Yang,[‡] and Yong-Ming Wei[‡]

[†]State Key Laboratory of Chemical Engineering, [‡]Membrane Science and Engineering R&D Center, Chemical Engineering Research Center, East China University of Science and Technology (ECUST), 130 Meilong Road, Shanghai 200237, China

Supporting Information

ABSTRACT: Polyethersulfone (PES)/perfluorosulfonic acid (PFSA) nanofiber membranes were successfully fabricated via electrospinning method from polymer solutions containing dispersed calcium carbonate ($CaCO_3$) nanoparticles. ATR-FTIR spectra indicated that the nanoparticles mainly existed on the external surface of the nanofibers and could be removed completely by acid treatment. Surface roughness of both the nanofibers and the nanofiber membranes increased with the $CaCO_3$ loading. Although FTIR spectra showed no special interaction between sulfonic acid ($-SO_3$) groups and $CaCO_3$ nanoparticles, XPS measurement demonstrated that the content of $-SO_3$ groups on external surface of the acid-treated nanofibers was enhanced by increasing $CaCO_3$ loading in solution. Besides, the acid-treated nanofiber membranes were performed in esterification reactions, and exhibited acceptable catalytic performance due to the activity of $-SO_3H$ groups on the nanofiber surface. More importantly, this type of membrane was very easy to separate and recover, which made it a potential substitution for traditional liquid acid catalysts.

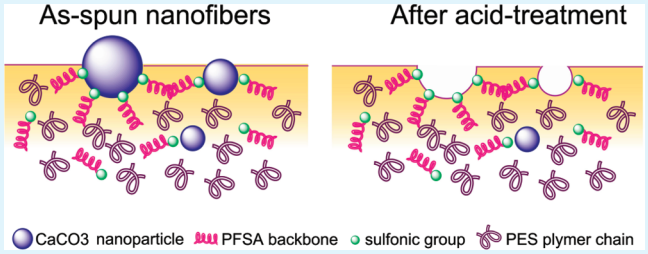

KEYWORDS: *electrospinning, nanofiber, polyethersulfone, perfluorosulfonic acid, $CaCO_3$ nanoparticle, catalytic activity*

1. INTRODUCTION

Perfluorosulfonic acid (PFSA) resin is a class of fluoro polymer consisting of a hydrophobic polytetrafluoroethylene (PTFE) backbone attached to hydrophilic sulfonic acid groups ($-SO_3$) via fluorocarbon polymer side chains (Figure 1).[1] Because of

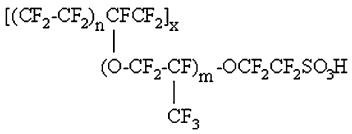

Figure 1. Chemical structure of PFSA molecule (m = 1–3; n = 67; $x \approx$ 1000).

the good chemical and thermal stability, especially the excellent ion-exchange capacity (IEC), PFSA membranes have broad prospects in present and potential applications. During the past three decades, PFSA resin has served as an important material for ion-exchange membrane in water electrolysis, chlor-alkali electrolyzers, organic synthesis reactions and also been widely studied in the fields of fuel cell membranes (FCM).[2−5] However, manipulation of purity PFSA into proton exchange membrane has been demonstrated of great difficulty because this polymer swells excessively in water (with a loss in mechanical properties and active acid sites) and is brittle when dry.[6] In consequence, great efforts have been made on development of composite materials to overcome these drawbacks. Therein, PFSA nanofiber membranes produced via electrospinning present outstanding performance due to their extremely high specific surface area (SSA) and excellent pore-interconnectivity structures, and have attracted scientific interest in these years. The carrier polymers in each nanofiber protect the membranes from swelling in water, providing the mechanical strength, and the high SSA ensures the optimum utilization of sulfonic acid groups.[6]

In recent years, scientific papers focused on electrospun PFSA nanofibers have increased greatly, and researches centering on structure control or property design of PFSA nanofibers for special applications are being explored by various methods. Impregnating electrospun nanofibers with appropriate amount of PFSA solution was proposed as an easy method to prepare functional membranes with sulfonic acid groups on the external surface.[7−9] Through this method, Molla et al.[10,11] prepared FCMs based on electrospun polyvinyl alcohol (PVA) membranes and reported good FCM performance of dimensional stability and low methanol crossover. However, functionalization through this method was only superficial and the membrane obtained was much lower in proton

Received: December 27, 2011
Accepted: March 7, 2012
Published: March 7, 2012

conductivity than pure PFSA.[11] Therefore, more attentions are being paid to direct electrospinning of PFSA blend solutions into nanofibers. Actually, it is the most common method in preparation and modification of PFSA nanofibers. Chen et al.[12] had detailed studies on electrospinning Nafion/poly(acrylic acid) (PAA) solutions and the results, similar to those in Choi's works,[13] showed that neat Nafion solution did not have adequate chain entanglement to successfully electrospin and smooth nanofibers could be produced only if PAA concentration was above 12 wt %. Recently, Nafion nanofiber-based polymer transducers were prepared by electrospinning Nafion solution with various polymers and subsequent hydrating with a specific ionic liquid.[14,15] The obtained nanofiber polymer transducers showed high speed of response. Laforgue et al.[16] prepared Nafion/polyethylene oxide (PEO) and Nafion/PVA nanofibers, and reported that the proton conductivity of these fiber membranes was slightly lower than that of conventional Nafion membranes. But Dong's research[17] demonstrated that high-purity Nafion (>99%) nanofibers with proton conductivity an order of magnitude higher than cast Nafion film could be successfully fabricated via electrospinning of Nafion/PEO solution. Dong suggested that these nanofibers could be applied as humidity sensors. More recently, Chang[18] had the first attempt to utilize electrospun PFSA/PVA nanofiber membranes as catalyst in esterification reaction of ethanol (EtOH) and acetic acid (HAc). Nevertheless, the results were not so satisfying. Besides, electrospinning PFSA solution doped with salt or nanotubes was also an effective method to expand and optimize the applications of this polymer. Lei[19] constructed Nafion/multiwalled carbon nanotube (MWCNT) nanofiber films as surface acoustic wave humidity sensor by electrospinning a solution with 5% Nafion, 2% MWCNT, and certain amount of polyvinyl pyrrolidone (PVP). The sensor achieved a remarkable improvement in RH sensitivity due to the existence of MWCNT which provided porous structure for Nafion. Similarly, nanofiber membranes with good ion removal capability of Cu^{2+} and Ca^{2+} in water were fabricated by Zhao et al.[20] with a solution of PFSA, PVP and a special organic disodium salt. However, electrospinning process of PFSA solution with metal, metal oxide, and inorganic salt nanoparticles, which should also have effects on the property and structure of electrospun nanofibers, were little reported in open literature.

In the present study, we reported the successful fabrication of polyethersulfone (PES)/PFSA nanofibers via electrospinning from polymer−$CaCO_3$ nanoparticle suspensions. After electrospinning, the $CaCO_3$ nanoparticles were removed by acid treatment. It was found that the incorporation of introduction−decomposition of $CaCO_3$ nanoparticles with the electrospinning process was a suitable approach to prepare nanofibers with rough surface and to further improve the surface area of the nanofibers. The $CaCO_3$ nanoparticles mostly gathered on the external surface of these nanofibers, and the interactions between $-CO_3$ and the $-SO_3$ were helpful to enhance the distribution of $-SO_3$ groups on the external surface. In addition, the nanofiber membranes were studied in the relationship of processing-structure−property and were tested in the reaction of ethanol and acetic acid. These nanofiber membranes showed good catalytic performance in this attempt, and the advantages such as easy separation and high recovery made them very attractive in this field.

2. EXPERIMENTAL SECTION

2.1. Materials and Suspension Preparation. PES (E3010, BASF) and PFSA-Na resin (prepared in laboratory, 1130EW, IEC=0.884 $mmol.g^{-1}$) were dissolved in N,N-dimethylacetamide (DMAc) at 60 °C with polymer concentration of 20 wt %, where m_{PES}:m_{PFSA} = 3:1. $CaCO_3$ nanoparticles (40−100 nm, spherical) were added into the solution with loading of 2, 4, 6, 8, and 10 wt %. The mixtures were scattered by ultrasonic treatment for 2 h and subsequently magnetic stirred at room temperature for 4 h. The shear viscosities of suspensions were measured using a Brookfield digital viscometer (DV-II+PRO, USA).

2.2. Electrospinning and Acid Treatment. The electrospinning setup (see the Supporting Information, Figure S1) used in this study was placed in the room with atmosphere condition of RH 40% and 20 °C. The electrospinning process lasted 20−25 h and the collected nanofiber membranes were 0.07−0.09 mm in thickness. These membranes were immersed in 1 M HCl solution for 48 h to ensure that the $CaCO_3$ nanoparticles on the surface were removed completely, and then washed by deionized water. Finally, the nanofiber membranes were dried in a vacuum oven for at least 24 h before further characterizations.

2.3. Characterization. To determine the morphology of the electrospun fibers, we observed the collected membranes under scanning electron microscope (SEM; JSM-6360LV, Japan) and atomic force microscope (AFM; NanoscopeIIIa, USA). The fiber diameters were then analyzed by Adobe Photoshop. Fourier transform infrared (FT-IR) spectra of the membranes were measured with a Nicolet spectrometer equipped with attenuated total reflectance (ATR) and an X-ray photoelectron spectroscopy analysis (XPS; VG-miclabII, UK) was utilized to determine the elemental composition of the external surface of the nanofibers. The specific surface area of the nanofiber membranes both before and after acid treatment was characterized by a N_2 adsorption instrument (JW-BK112F, China). To determine the mechanical property of the acid-treated nanofiber membranes, the specimens were prepared by cutting the nanofiber membranes into rectangular shape with a planar dimension of width × length = 5 mm × 30 mm. The tensile testing was performed using a universal testing machine (QJ210A, China) with a common used cross-head speed of 10 mm/min at room temperature.[21−23]

3. RESULTS AND DISCUSSION

3.1. Suspension Viscosity. Viscosity was regarded as the one of the key parameters in electrospinning process.[24] In this study, the shear viscosity was sensitive to $CaCO_3$ loading because the nanoparticles were not really dissolved in DMAc, where only suspensions formed. As indicated in Figure 2, the shear viscosities increased with $CaCO_3$ loading from 2 to 10 wt. %, but decreased with shear rates. Specifically, the viscosity of the 2 wt % $CaCO_3$ solution (labeled as S-2 in Figure 2, similarly hereinafter) was 884, 622, and 586 cP at shear rates of 0, 50, and 100 s^{-1}, respectively. As Comparison, the 10 wt % $CaCO_3$ solution exhibited the viscosities 1400, 650, and 600 cP higher at each shear rate, respectively.

Previous research has provided evidence that the viscosity response of nanoparticle− polymer solution resulted from frictional interactions between the nanoparticles[25] and between the polymer chains and nanoparticles.[26] Therefore, it was easy to understand that the viscosity of the suspension increased

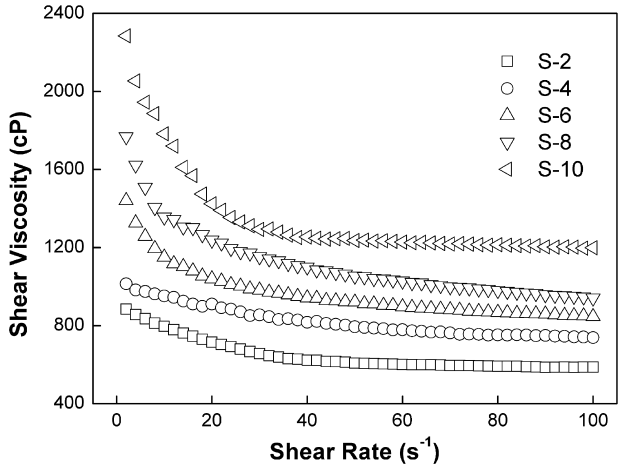

Figure 2. Viscosities of the $CaCO_3$ nanoparticle-PES/PFSA solutions (25 °C).

with $CaCO_3$ loading because eof the enhancement in the frictional interaction in system. The change of the viscosity of the suspension with shear rate could be explained as follows (see Figure 3): $CaCO_3$ nanoparticles formed agglomerations,

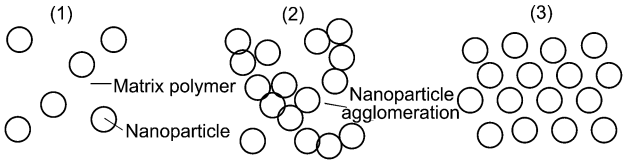

Figure 3. Idealized view of the effects of nanoparticle dispersion on the viscosity of the nanoparticle- polymer solutions: (1) nanoparticles do not overlap at low content; (2) nanoparticle agglomerations occurred at high content and enhanced the frictional interactions; (3) high-frequency shear action reduced the nanoparticle agglomerations and resulted in a uniform dispersion of the nanoparticles.[26].

especially at high loading due to the action of surface energy. These agglomerated nanoparticles caused excess frictional interactions, which further enhanced the shear viscosity. However, shearing action would disrupt the agglomerations and make the nanoparticles in uniform dispersion. As a result, the shear viscosity decreased rapidly with the shear rate at low frequencies,[27] especially at high loading, but exhibited relatively smooth changes at high shear rates.

3.2. Morphology. At $CaCO_3$ loading of 2 wt %, smooth nanofibers were easily fabricated and collected, as shown in Figure 4(1). The nanofibers had a narrow diameter distribution from 80 to 250 nm with an average value, d = 164 nm (see the Supporting Information, Figure S2). While increasing $CaCO_3$ loading, thicker nanofibers with wider diameter distribution were produced because of the increase in viscosity of the polymer−nanoparticle suspensions. Average diameter of nanofibers from 6 and 10 wt % $CaCO_3$ suspensions was 192 and 245 nm, respectively. Besides, nanoparticle agglomerations were observed on the surface of nanofibers, as shown in Figure 4(2) and Figure 4(3). As described previously, nanoparticle agglomerations occurred at high $CaCO_3$ loading, and these agglomerations would gather on the surface of the nanofibers after electrospinning.

After acid treatment, the exposed nanoparticles were removed completely, leaving pits and pores on the surface as indicated in Figure 4(4, 5, and 6). AFM images of the nanofiber membranes were given in Figure 5(left). Surface roughness of these membranes increased with nanofiber diameter and was 30.4, 35.5, 132.1, and 199.7 nm for membrane M-0 (the membrane electrospun from the suspension with 0 wt.% $CaCO_3$, similarly hereinafter), M-2, M-6, and M-10, respectively. However, for single nanofibers, the surface change was much different. As shown in Figure 5(right), the nanofibers of membrane M-2 had smooth profile curve along the axis and possessed the surface roughness of 7.3 nm. As Comparison, the nanofibers in membrane M-6 and M-10 had surface roughness of 10.5 nm and 19.1 nm, respectively. Furthermore, the profile curve of the nanofibers in membrane M-10 exhibited many irregular dentate shapes, which meant the occurrence of rough structures. That might be the pits and pores resulted from the $CaCO_3$ nanoparticles on the fiber surface, and these structures would have effects on surface properties of the nanofiber membranes e.g., hydrophilicity nature and specific surface area.

3.3. Structural Property. Water contact angle (WCA) was measured as one of the properties to determine the surface structure of the electrospun nanofiber membranes. A distilled water pendent droplet was injected from a syringe onto the membrane surface. The image of the droplet on the membrane was visualized through the image analyzer and the angle between the water droplet and the surface was measured. As

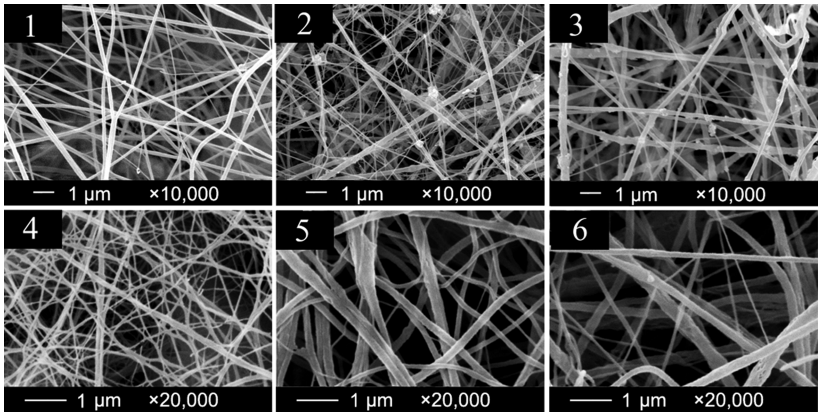

Figure 4. SEM images of the nanofibers: (1−3) as-spun nanofibers from 2, 6, and 10 wt % $CaCO_3$ suspensions; (4−6) the above nanofibers after acid treatment.

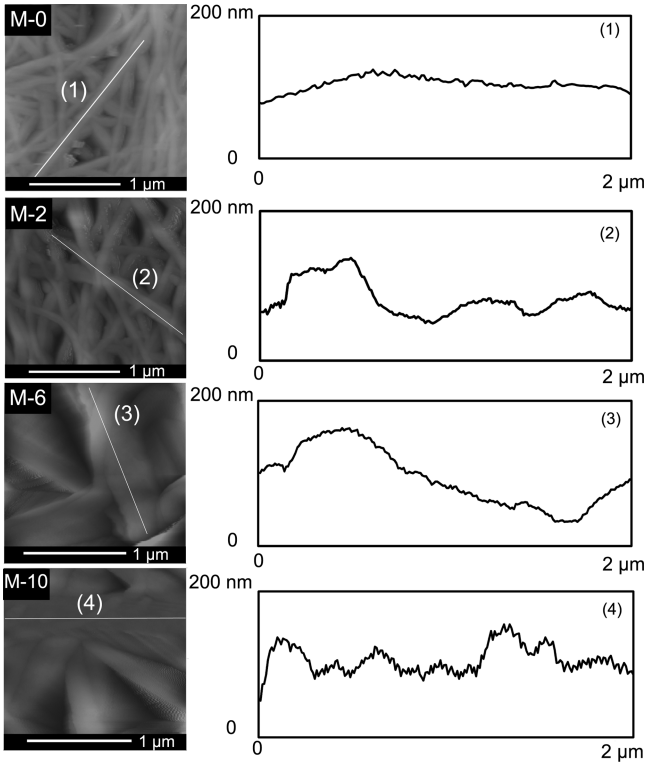

Figure 5. AFM images of the nanofiber membranes after acid treatment (left), and the height profiles of the single nanofiber along the axis (right).

illustrated in Figure 6, the as-spun nanofiber membranes presented strong hydrophobicity initially. WCA of membrane

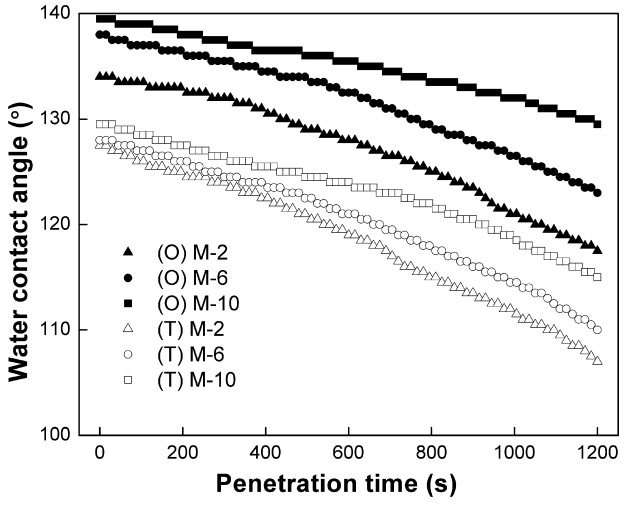

Figure 6. Time-dependent WCAs of the nanofiber membranes: (O) the as-spun nanofiber membranes; (T) the nanofiber membranes after acid treatment.

M-10 was 139° at t = 0 min, whereas membrane M-2 exhibited a smaller value of 133.5°. Obviously, WCAs of the membranes from high $CaCO_3$ loading suspensions were greater than those of the membranes from low $CaCO_3$ loading suspensions either before or after acid treatment. This difference could be attributed to the enhancement of the surface roughness. It was proposed mathematically and experimentally that WCA was increased by roughness, whereas θ was greater than 90°.[28]

As mentioned above, increase in $CaCO_3$ loading resulted in the nanofiber membranes with greater surface roughness, which led to higher WCAs.

Moreover, it was apparent in Figure 6 that the WCAs of the nanofiber membranes reduced 10° or thereabout after acid treatment. A conjecture was proposed that the decrease in WCAs was resulted from the enhancement of $-SO_3$ groups on the nanofiber surface. Since $CaCO_3$ nanoparticle was a type of polar filler with large amount of C═O bonds exposed on the surface[29] and PFSA resin also had strong polar groups at the end of the polymer chains, this polymer, in great probability, would have interactions with the nanoparticles. After electrospinning, there were plenty of $CaCO_3$ nanoparticles on the surface of the as-spun nanofibers. As the nanoparticles were removed by acid treatment, the $-SO_3$ groups interacted with them would be exposed on the surface, as illustrated in Figure 7. These groups significantly increased the hydrophilicity and

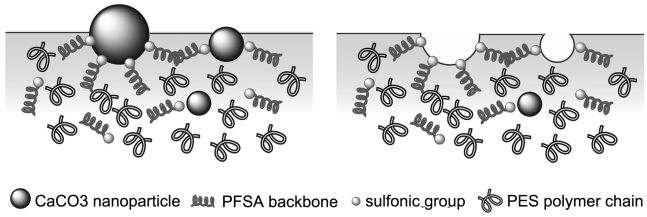

Figure 7. Schematic diagram of a single nanofiber before (left) and after (right) acid treatment.

led to the decrease in WCAs of the nanofiber membranes after acid treatment.

To prove the conjecture and examine the interactions between the polymer and nanoparticles in the electrospun nanofiber membranes, ATR-FTIR was employed with three different thin samples and the corresponding spectra ranging from 2000 to 650 cm^{-1} were shown in Figure 8. Obvious

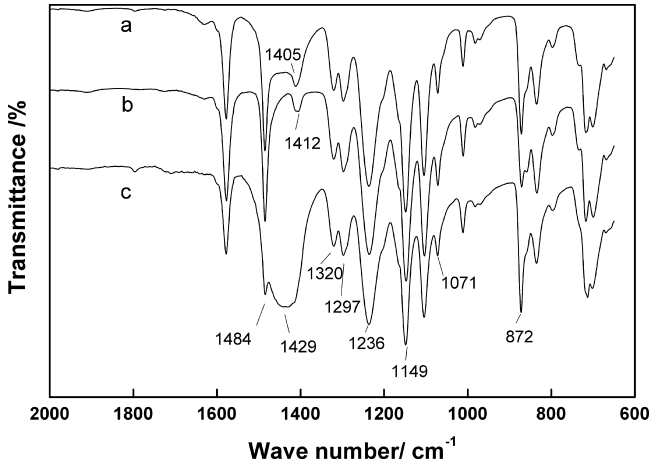

Figure 8. ATR-FTIR spectra of the PES/PFSA/$CaCO_3$ membranes: (a) cast membrane (b) nanofiber membrane after acid treatment, (c) as-spun nanofiber membrane.

differences could be observed at 872 cm^{-1} and in 1405−1484 cm^{-1}. The broad peak at 1429 cm^{-1} in Figure 8c was the characteristic absorption of $-CO_3$, which decreased significantly in Figure 8a. This variation indicated that the $CaCO_3$ nanoparticles much gathered on the surface of the nanofibers, but distributed uniformly in the cast film, attributed to the

dx.doi.org/10.1021/am201843y | ACS Appl. Mater. Interfaces 2012, 4, 1716−1723

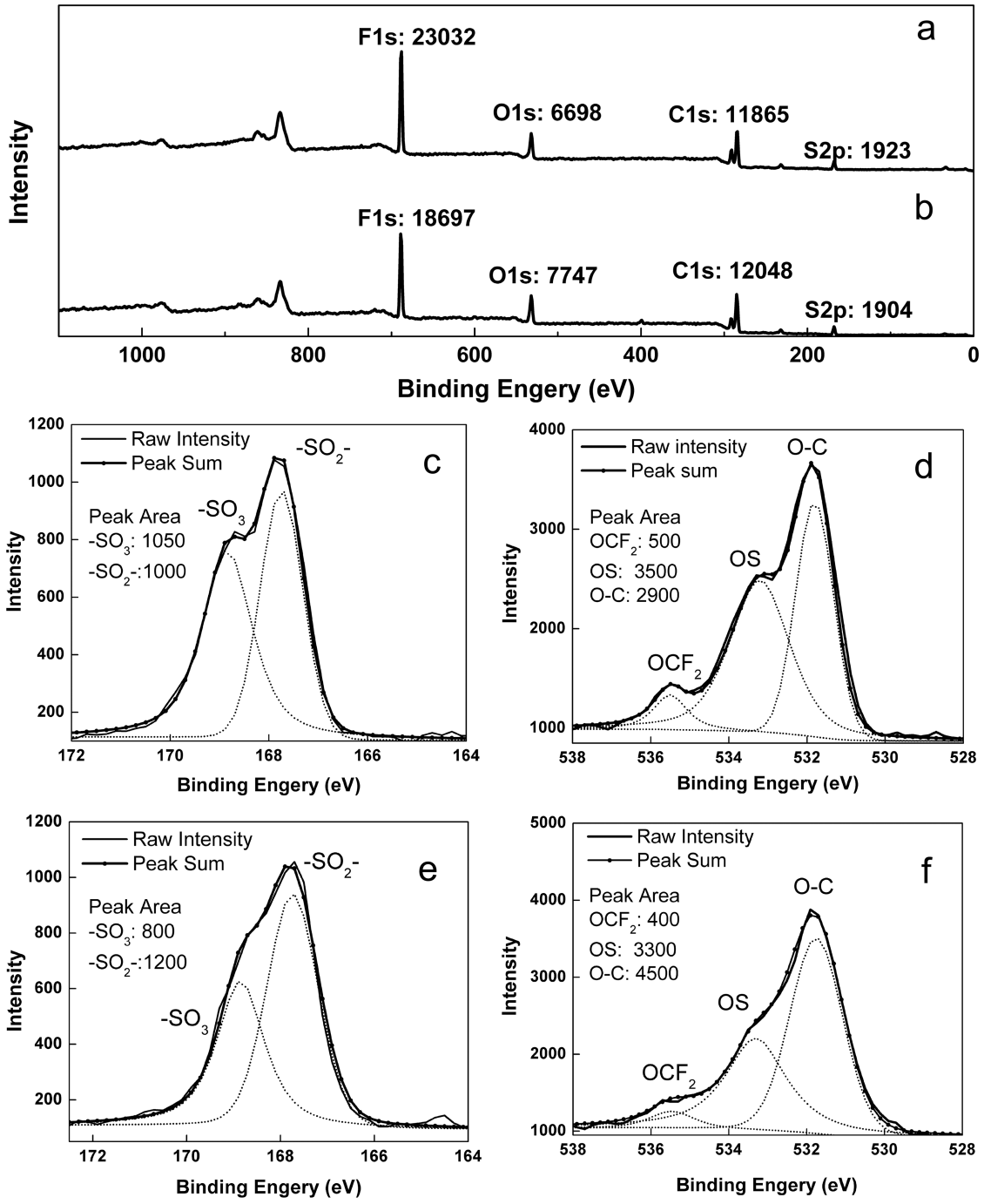

Figure 9. XPS spectra of electrospun membranes (a) peak areas of each element in membrane M-10, (b) peak areas of each element in membrane M-2, (c) S2p region of M-10, (d) O1s region of M-10, (e) S2p region of M-2, (f) O1s region of M-2.

instability in electrospinning process and the small size of the nanofibers in which $CaCO_3$ nanoparticles could be hardly encapsuled. Moreover, the strong peak disappeared in Figure 8b, which suggested that the $CaCO_3$ nanoparticles were removed completely after acid treatment.

Besides, the peaks near 1320 and 1297 cm^{-1} were attributable to asymmetric stretching of $-SO_2-$ groups in PES and the strong peaks in 1236 and 1155 cm^{-1} were corresponding to $-CF_2-$ groups in PFSA.[30] The peaks at 1071 cm^{-1} were due to the stretching of the $-SO_3$ groups. Through these characteristic peaks, it was confirmed that the original chemical structures of PES and PFSA were not affected by high voltage. But unfortunately, not any special interaction between the polymer and nanoparticles was observed from the spectra.

However, some interesting results were observed while referencing to surface elemental composition characterized by XPS analysis. There was an obvious increase in fluorine content and a corresponding decrease in oxygen content as comparing membrane M-2 with M-10, as shown in panels a and b in Figure 9. These changes could be attributed to the increase in PFSA backbones distributed on the external surface of the electrospun nanofibers, associated with the increase of $CaCO_3$ nanoparticle loading. Though the sulfur content did not show

significant changes, the results of the detailed elemental composition provided by the spectra of the sulfur region indicated that the content of sulfur elements in different chemical environment changed much with $CaCO_3$ loading. The XPS signal observed in S2p region at 168.9 eV was attributed to $-SO_3$ in PFSA molecule and that at 167.7 eV was attributed to $-SO_2-$ in PES molecule. The sulfur content of $-SO_3$, as shown in Figure 9c, was close to that of $-SO_2-$ in membrane M-10, but much lower than $-SO_2-$ in membrane M-2, in Figure 9e). This result suggested that the content of $-SO_3$ groups on the nanofiber surface in membrane M-10 was greater than that in M-2 since the total amount of sulfur content did not change much. Meanwhile, the spectra of O1s region showed the variation tendency consisted with above results. Specifically, the signal at 531.9 eV could be attributed to the ether oxygen in PES molecule (labeled as O−C), and the signals at 533.1 and 535.6 eV belonged to $-SO_3$ (or $-SO_2-$) (labeled as OS) and ether oxygen in PFSA molecule and (labeled as OCF_2), respectively. The decrease in O−C content (peak area: 2900 of M-10 in Figure 9d and 4500 of M-2 in Figure 9)) was attributed to the decrease in PES backbones on the nanofiber surface, associated with the increase in $CaCO_3$ loading. However, OS content did not change much though the $-SO_2-$ content decreased due to the decrease in PES content, which suggested that there must be an enhancement of the $-SO_3$ groups on the surface. Thus, it could be considered that increase of $CaCO_3$ nanoparticle loading was beneficial to improve the distribution of $-SO_3$ groups on the nanofiber surface.

N_2 physical sorption performed on the membranes quantified the specific surface area (SSA) of the membranes before and after acid treatment, and provided further evidence for the morphology observed by SEM and AFM.

Theoretically, SSA of the membrane is susceptive to the diameter of the nanofibers based on the relationship described by the following equation

$$\mathrm{SSA} = \frac{A}{m} = \frac{\pi dl}{\rho \pi l d^2/4} = \frac{4}{\rho d}$$

where ρ is the density of the polymer and d refers to the diameter of the single nanofiber. However, linear decrease in SSA did not appear with the increase of nanofiber diameter, as shown in Table 1. Instead, the SSA(O) presented only slight decrease with diameter and even the SSA(T) remained almost unchanged for various membranes. Because $CaCO_3$ nanoparticles used in this study had large specific surface area, SSA of the as-spun membranes would be improved by increasing $CaCO_3$ loading, which largely offset the impact of increase in nanofiber diameter. Thus, the SSA(O) only showed slightly decrease with $CaCO_3$ loading. For the acid-treated membranes, the nanoparticles were removed completely, leaving pits or pores on the surface, which further improved SSA of the membranes, resulting in the invariableness in SSA(T). Moreover, for a given membrane, either the SSA(O) or the SSA(T) was much greater than SSA(C). Especially, for membrane M-10, the SSA(T) was 72.6% larger than SSA(C) and 23.7% larger than SSA(O), which suggested the immense existence of rough structures on the acid-treated membrane surface. In this way, it could be concluded that the addition-and-removing of the $CaCO_3$ nanoparticles was helpful to produce nanofibers with rough surface and improve SSA of the nanofiber membranes. These rough structures also had significant effects on the mechanical properties of the nanofiber membranes as described below.

Table 1. SSA of Different Membranes (Values Given Were Averaged from Three Measuring Results)

no.	mean diameter (nm)	SSA(O)[a] (m^2/g)	SSA(T)[b] (m^2/g)	SSA(C)[c] (m^2/g)
M-0	155	20.6 ± 0.33	20.9 ± 0.16	19.1
M-2	164	19.3 ± 0.21	21.7 ± 0.23	18.5
M-6	192	18.1 ± 0.15	21.5 ± 0.19	15.8
M-10	245	17.3 ± 0.16	21.4 ± 0.15	12.4

[a]SSA(O): specific surface area of the as-spun membrane. [b]SSA(T): specific surface area of the acid-treated membrane. [c]SSA(C): specific surface calculated from the mathematical formula.

Mechanical characterization in this research was achieved by applying tensile test loads to rectangular specimens of ultrafine nonwoven fiber membranes since the single polymer nanofiber was too weak. The stress−strain behaviors of the acid-treated nanofiber membranes are shown in Figure S3 in the Supporting Information, and the stress at break and the resulting modulus for each sample are summarized in Table 2. As a whole, the tensile strength and modulus of the membranes increased with $CaCO_3$ loading. Specifically, nanofiber membrane M-2 was very weak, with stress at break, σ_t of around 0.3 MPa and the elastic modulus, E_t of 1.16 MPa. In contrast, nanofiber membrane M-10 exhibited much higher stress at break of 1.88 MPa and an even greater modulus of 19.9 MPa. However, this increase in strength was not absolute. The break strength of M-8 was much larger than that of M-2 but a little less than that of M-6, and similarly for the Young's modulus. So far, there were no strict rules of the mechanical property change for disorderly arranged electrospun nanofibers. In this study, break strength of the membranes only showed a general trend of increase with $CaCO_3$ loading. This trend could be attributed to the interactions between the nanofiber networks, associated with the surface roughness of the nanofibers. Because the surface roughness of the nanofibers was increased by $CaCO_3$ loading, it improved the frictional resistance between the nanofibers and enhanced the connection of the nanofiber networks.[22] Thus the applied stress could be readily transferred to the entire nanofiber network from local position and therefore, the stress at break of the nanofiber membrane was greatly improved. Meanwhile, the stretch ratio of the nanofiber membranes decreased from 40 to 9% while $CaCO_3$ loading increased from 2 to 8 wt %. It could be easily understood that the frictional resistance between the nanofibers restricted the mobility of the nanofiber network and resulted in the decrease of the elongation of the membranes. But an unexpected increase to 21% in stretch ratio was found in membrane M-10. A

Table 2. Mechanical Property of the Nanofiber Membranes after Acid Treatment (values given were averaged from three samples)

No.	$CaCO_3$ loading wt %	break strength σ_t (MPa)	elongation at break ε_t (%)	Young's modulus E_t (MPa)
M-2	2	0.30 ± 0.04	40 ± 4.0	1.16 ± 0.08
M-4	4	0.27 ± 0.03	30 ± 3.3	1.26 ± 0.11
M-6	6	0.87 ± 0.05	22 ± 3.6	10.30 ± 0.85
M-8	8	0.69 ± 0.02	9 ± 1.8	9.22 ± 0.73
M-10	10	1.88 ± 0.11	21 ± 2.6	19.9 ± 1.39

dx.doi.org/10.1021/am201843y | ACS Appl. Mater. Interfaces 2012, 4, 1716−1723

reasonable explanation was that the pattern formation of membrane M-10 was much different from the others. Actually, for electrospun nanofiber membranes, tensile properties were more related to the assemblies of the nanofibers such as the pattern of the nanofibers than the physical linking and the frictional entanglements between the nanofibers,[22] etc. Unfortunately, theoretical or empirical models have rarely been reported up to now.

3.4. Catalytic Performance. The catalytic performance of the collected nanofiber membranes was evaluated in an esterification reaction (EtOH:HAc:PFSA = 6 mol:3 mol:1 g). The reaction was carried out at 75 °C for 8 h and the results were shown in Figure 10.

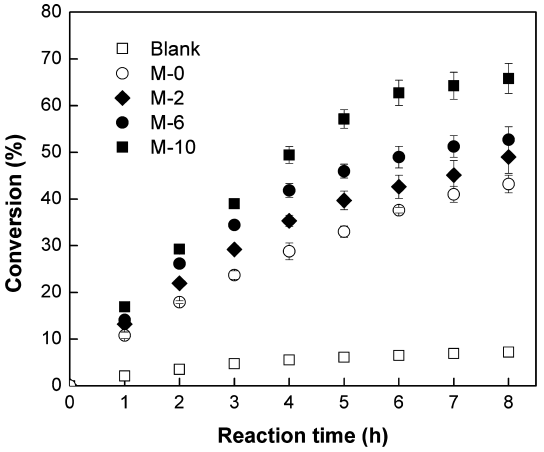

Figure 10. Conversion rate of ethyl acetate in the esterification reaction as a function of time.

As expected from the XPS results, the catalytic performance of the nanofiber membranes would increase from M-2 to M-10 due to the enhancement of $-SO_3H$ groups on the membrane surface. It was found that the esterification reaction hardly occurred without catalyst. But as PES/PFSA nanofiber membrane was employed, the reaction rate was greatly improved because of the catalytic activity of $-SO_3H$ groups. The nanofiber membranes provided large surface area and inner porosity (>90%) so that the EtOH and HAc could easily attach to the reaction sites. As a result, nanofiber membrane M-10, which had most $-SO_3H$ groups on the surface, presented the best catalytic performance. Specifically, by using nanofiber membrane M-10, the conversion rate of HAc achieved 68% within 8 h, which was approximately 10 times higher than that without catalyst. This conversion was lower than but comparable to the result of conventional catalyst (98% H_2SO_4, 75% for HAc).

After reaction, the nanofiber membranes were recycled by filtration and oven drying. The weighing results showed that the membranes obtained were almost of the same mass as those before reaction (recovery rate >99.5% in each case). Thus, this kind of nanofiber membranes could be a potential substitution for some conventional liquid-acid catalyst, which was difficult to be separated in homogeneous reactions.[3,18]

4. CONCLUSIONS

In this work, PES/PFSA nanofibers were successfully fabricated via electrospinning of polymer-$CaCO_3$ nanoparticle solutions. These nanofiber membranes presented high specific surface area, which was more than 70% improved by introduction-and-removing of $CaCO_3$ nanoparticles. Moreover, the content of $-SO_3$ groups on the nanofiber surface was enhanced likely due to the interaction between CO_3^{2-} and $-SO_3$. And this could be an effective and universal method to improve the utilization of the active groups of PFSA in many other applications. Besides, the produced nanofiber membranes were tested in esterification reactions of ethanol and acetic acid, and exhibited acceptable catalytic performance. Furthermore, the ease of separation and very high recovery make them a potential material that could serve in acid-catalytic reactions.

■ ASSOCIATED CONTENT

Supporting Information

Details of the experimental setup, the diameter distribution, and the stress−strain behaviors of the acid-treated nanofiber membranes. This material is available free of charge via the Internet at http://pubs.acs.org/.

■ AUTHOR INFORMATION

Corresponding Author

*E-mail: chemxuzl@ecust.edu.cn. Tel: 86-21-64253061. Fax: 86-21-64252989.

Notes

The authors declare no competing financial interest.

■ ACKNOWLEDGMENTS

The authors thank the Key Technology R&D Program of China (20092 × 02032) for financial support. The authors are grateful to Dr. Dong-gen Chen for help with the measurement of SEM pictures of these nanofibers.

■ REFERENCES

(1) Mauritz, K. A.; Moore, R. B. *Chem. Rev.* **2004**, *104*, 4535−4586.
(2) Yeo, R.; McBreen, J.; Kissel, G.; Kulesa, F.; Srinivasan, S. *J. Appl. Electrochem.* **1980**, *10*, 741−747.
(3) Gelbard, G. *Ind. Eng. Chem. Res.* **2005**, *44*, 8468−8498.
(4) Neburchilov, V.; Martin, J.; Wang, H.; Zhang, J. *J. Power Sources* **2007**, *169*, 221−238.
(5) Carla, H. W. *J. Membr. Sci.* **1996**, *120*, 1−33.
(6) Choi, J.; Lee, K. M.; Wycisk, R.; Pintauro, P. N.; Mather, P. T. *Macromolecules* **2008**, *41*, 4569−4572.
(7) Choi, S.; Fu, Y. Z.; Ahn, Y.; Jo, S.; Manthiram, A. *J. Power Sources* **2008**, *180*, 167−171.
(8) Lin, H. L.; Wang, S. H.; Chiu, C. K.; Yu, T. L.; Chen, L. C.; Huang, C. C.; Cheng, T. H.; Lin, J. M. *J. Membr. Sci.* **2010**, *365*, 114−122.
(9) Shabani, I.; Hasani-Sadrabadi, M. M.; Haddadi-Asl, V.; Soleimani, M. *J. Membr. Sci.* **2011**, *368*, 233−240.
(10) Molla, S.; Compan, V. *J. Membr. Sci.* **2011**, *372*, 191−200.
(11) Molla, S.; Compan, V.; Gimenez, E.; Blazquez, A.; Urdanpilleta, I. *Int. J. Hydrogen Energy* **2011**, *36*, 9886−9895.
(12) Chen, H.; Snyder, J.; Elabd, Y. *Macromolecules* **2008**, *41*, 128−135.
(13) Choi, J.; Wycisk, R.; Zhang, W. J.; Pintauro, P. N.; Lee, K. M.; Mather, P. T. *Chemsuschem* **2010**, *3*, 1245−1248.
(14) Akle, B.; Leo, D. J.; Nah, C.; Kader, A. M. *Mater. Res. Soc. Symp. Proc.* **2006**, *889*, 85−90.
(15) Nah, C.; Lee, Y.; Cho, B.; Yu, H.; Akle, B.; Leo, D. *Compos. Sci. Technol.* **2008**, *68*, 2960−2964.
(16) Laforgue, A.; Robitaille, L.; Mokrini, A.; Ajji, A. *Macromol. Mater. Eng.* **2007**, *292*, 1229−1236.
(17) Dong, B.; Gwee, L.; Salas-de la Cruz, D.; Winey, K. I.; Elabd, Y. A. *Nano Lett.* **2010**, *10*, 3785−3790.
(18) Chang, X. F.; Hu, Y.; Xu, Z. L. *Mater. Lett.* **2011**, *65*, 1719−1722.

(19) Lei, S.; Chen, D. J.; Chen, Y. Q. *Nanotechnology* **2011**, 22.
(20) Zhao, J. H.; Yuan, W. Z.; Xu, A. H.; Ai, F.; Lu, Y. W.; Zhang, Y. M. *React. Func. Polym.* **2011**, *71*, 1102−1109.
(21) Fujihara, K.; Kotaki, M.; Ramakrishna, S. *Biomaterials* **2005**, *26*, 4139−4147.
(22) Lee, K. H.; Kim, H. Y.; Ryu, Y. J.; Kim, K. W.; Choi, S. W. *J. Polym. Sci., Part B: Polym. Phys.* **2003**, *41*, 1256−1262.
(23) Huang, Z. M.; Zhang, Y.; Ramakrishna, S.; Lim, C. *Polymer* **2004**, *45*, 5361−5368.
(24) Zhao, J. H.; Xu, A. H.; Yuan, W. Z.; Gao, J. B.; Tang, J. K.; Wang, L.; Ai, F.; Zhang, Y. M. *J. Mater. Sci.* **2011**, *46*, 7501−7510.
(25) Cassagnau, P. *Polymer* **2008**, *49*, 2183−2196.
(26) Rothon, R. N.; Hancock, M. General Principles Guiding Selection and Use of Particulate Materials. In *Particulate-Filled Polymer Composites*; Rothon, R. N., Ed.; Rapra Technology Limited: Shrewsbury, U.K., 2003; p 34−35.
(27) Karamipour, S.; Ebadi-Dehaghani, H.; Ashouri, D.; Mousavian, S. *Polym. Test.* **2011**, *30*, 110−117.
(28) Adamson, A. W.; Gast, A. P., The solid−liquid interface contact angle. *Physical Chemistry of Surfaces*, 6th ed; Wiley: New York, 1997; pp 358−359.
(29) Kalaee, M.; Akhlaghi, S.; Nouri, A.; Mazinani, S.; Mortezaei, M.; Afshari, M.; Mostafanezhad, D.; Allahbakhsh, A.; Dehaghi, H. A.; Amirsadri, A. *Prog. Org. Coat.* **2011**, *71*, 173−180.
(30) Gruger, A.; Régis, A.; Schmatko, T.; Colomban, P. *Vib. Spectrosc* **2001**, *26*, 215−225.